Simultaneous Diffraction of X Rays and the Borrmann Effect*

EDWARD J. SACCOCIO† AND ALFRED ZAJAC‡
Physics Department, Polytechnic Institute of Brooklyn, Brooklyn, New York
(Received 15 February 1965)

The Borrmann effect (the anomalous transmission of x rays through thick perfect crystals) has been used as the primary diffraction in a study of simultaneous diffraction. The major part of the work is an analysis of multiple diffraction using the dynamical theory of x-ray diffraction. In the analysis we have utilized the concept of normal modes in describing the propagation of the x-ray wave field. We have determined these modes when the Bragg condition is exactly and simultaneously satisfied for all the diffracting planes. The particular configuration studied was one in which only three noncoplanar waves have appreciable amplitudes. We have shown that at least one of the proper modes of any three-field case of the type considered is a nonabsorbing mode of propagation (i.e., having nodes of the electric field at the atomic planes). This indicates that the primary anomalous transmission will persist with little or no change in intensity when a third reciprocal lattice point enters the Ewald sphere. In particular, when the third reciprocal lattice point is of the same family as the primary, simultaneous anomalous transmission is predicted. For this case, a relatively small change in the primary reflected beam and a twofold enhancement of the forward beam is calculated which are seen to be due to a superposition of two degenerate Borrmann effects having a common forward diffraction direction. Experimental results using polarized and unpolarized incident radiation are presented and discussed.

1. INTRODUCTION

THE anomalous transmission of x rays through perfect or almost perfect crystals (also called the Borrmann effect) was discovered some twenty years ago. Crystal plates which are thick enough to absorb all of the incident x-ray radiation will transmit the diffracted x rays when the beam is incident at or close to a Bragg angle. In addition, a characteristic feature of the effect is that two beams appear on the far side of the crystal plate [Fig. 1(a)]. That this anomalous transmission is possible is due to the fact that the usual absorption is considerably diminished by a system of standing waves which are set up in the crystal, some of which have nodes in the atomic planes. A considerable number of experimental investigations exploring anomalous transmission have been reported in the literature wherein the results are necessarily explained in terms of the dynamical theory of x-ray diffraction.[1–5]

In this study we have undertaken an experimental and theoretical investigation of situations in which more than one set of atomic planes are in position to transmit anomalously. Figure 1(b) shows one case when two sets of atomic planes are in position for the diffraction of the same incident beam (shown as coplanar, for convenience). If anomalous transmission can be exhibited separately for each set of these planes, then together we might expect simultaneous anomalous transmission. An explanation of such multiple diffraction requires the use of the dynamical theory. The very general principles of the dynamical theory of x-ray diffraction were formulated by Ewald and Laue and they deal with any number of diffractions. All the factors affecting intensity such as crystal structure, temperature, the polarization of the incident x-ray beam, and others, have been determined only for that case when one set of planes diffracts. It is understood

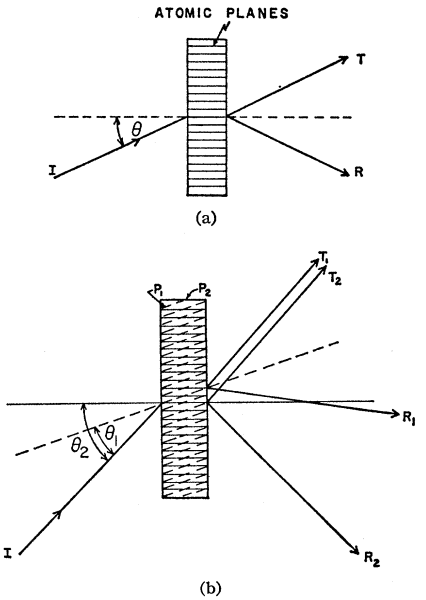

FIG. 1. (a) Anomalous transmission. I—incident x-ray beam, θ—Bragg angle, T—anomalous transmitted beam, R—anomalous reflected beam. (b). Simultaneous anomalous transmission. I—Incident x-ray beam, $\theta_1\theta_2$—Bragg angles for atomic planes P_1P_2, T_1T_2—anomalous transmitted beams, R_1R_2—anomalous reflected beams.

* Submitted in partial fulfillment of the requirements for the Ph.D. degree in the Department of Physics at the Polytechnic Institute of Brooklyn. This research was supported by a grant from the National Science Foundation.

† Present address: Physics Department, St. John's University, Jamaica, New York.

‡ Present address: Department of Physics, Adelphi University, Garden City, New York.

[1] W. H. Zachariasen, *Theory of X-Ray Diffraction in Crystals* (John Wiley & Sons, Inc., New York, 1946).

[2] R. W. James, *The Optical Principles of the Diffraction of X-Rays* (G. Bell and Sons, London, 1950).

[3] R. W. James, in *Solid State Physics*, edited by F. Seitz and D. Turnbull (Academic Press Inc., New York, 1963), Vol. 15, pp. 55–222.

[4] N. Kato, Acta Cryst. **11**, 885 (1958).

[5] B. Batterman and H. Cole, Rev. Mod. Phys. **36**, 681 (1964).

why this detailed theory was not readily extended to multiple diffraction. In any case when one set of atomic planes causes diffraction, the incident beam together with the reflected form a single plane which serves as a reference plane to specify, by parallel and perpendicular components, the electric intensity vector. In addition, it is reasonably simple to obtain the equations of the dispersion sheets from which practically all the properties of the wavefields can be obtained. None of this is in general true for multiple diffraction. When there are more than one set of diffracting planes it is very difficult to deal with the equations of the dispersion sheets. We handled this latter difficulty by considering the instance when all the atomic planes involved in the simultaneous diffraction are inclined exactly at Bragg angles, i.e., we used only the diameter points of the dispersion sheets. We also realized that the proper solution of the problem requires the evaluation of the normal modes of propagation of the electromagnetic waves which are propagated through the crystal. Having obtained the modes of propagation (for the diameter points of the dispersion sheets) we were able to predict which of the modes would be anomalously transmitted through thick perfect crystals.

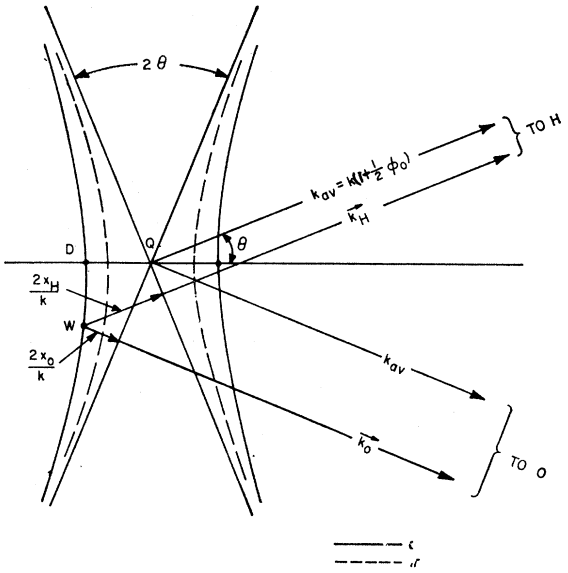

FIG. 2. Dispersion curves in single diffraction. Point Q is the center of the sphere of reflection or the intersection of circles drawn from reciprocal points O and H. In the scale of this figure these circles appear as straight lines (O is of the order of one mile from Q).

2. THEORY

2.1. General Theory

The general dynamical theory of x-ray diffraction developed by Ewald[6] and Laue[7] has been subsequently discussed by many authors.[1–5] With a plane monochromatic x-ray wave incident, the solutions of Maxwell's equations inside a crystal are assumed to consist of a superposition of plane waves, and thus the electric-displacement-field vector $\mathbf{D}$ will be of the form

$$\mathbf{D}=e^{i\nu t}\sum_{n=-\infty}^{+\infty}\mathbf{D}_n e^{-i\mathbf{k}_n\cdot\mathbf{r}}, \tag{2.1}$$

where $\mathbf{k}_n$ is the wave vector directed towards the nth reciprocal lattice point. The directions of the electric vectors are transverse to the respective directions of propagation, and for every wave vector $\mathbf{k}_n$ the corresponding electric vector $\mathbf{D}_n$ will be described completely by its components $D_n{}^\sigma$ and $D_n{}^\pi$ along the axes specified by two unit transverse vectors $\boldsymbol{\sigma}_n$ and $\boldsymbol{\pi}_n$.

The condition of the self-consistency of the wave fields inside the crystal is expressed by the equations[4]

$$\begin{aligned}-x_n D_n{}^\sigma&=\sum_{r=-\infty}^{+\infty}{}'\,\phi_{n-r}[D_r{}^\sigma(\boldsymbol{\sigma}_n\cdot\boldsymbol{\sigma}_r)+D_r{}^\pi(\boldsymbol{\sigma}_n\cdot\boldsymbol{\pi}_r)],\\ -x_n D_n{}^\pi&=\sum_{r=-\infty}^{+\infty}{}'\,\phi_{n-r}[D_r{}^\sigma(\boldsymbol{\pi}_n\cdot\boldsymbol{\sigma}_r)+D_r{}^\pi(\boldsymbol{\pi}_n\cdot\boldsymbol{\pi}_r)],\end{aligned} \tag{2.2}$$

where x_n is defined by the relation

$$k^2x_n=k_n{}^2-k^2(1-\phi_0), \tag{2.3}$$

and has the geometric meaning indicated in Fig. 2[8]; $\mathbf{k}$ is the vacuum value of the wave vector and ϕ_m is the Fourier component of the polarizability and is given by

$$\phi_m=A\sum f_j e^{-2\pi i\mathbf{m}\cdot\mathbf{r}}$$

or

$$\phi_m=AF_m,$$

i.e., ϕ_m is proportional to the geometrical structure factor.

Out of the infinite number of component waves, when q reciprocal lattice points are close to the Ewald sphere, only q wave components will have appreciable amplitudes; in such a case in Eqs. (2.2) $n=1, 2, \cdots, q$. Usually $q=2$, and this corresponds to ordinary single diffraction. In this paper we will extend the theory to multiple diffraction, i.e., to the case when q is greater than two.

The condition that the homogeneous equations (2.2) have nontrivial solutions yields a determinantal equation in the x_n's which is the familiar dispersion surface in reciprocal space. When q reciprocal lattice points are on the Ewald sphere, the order of the equation is $2q$, and it then represents $2q$ dispersion sheets. For any one point on one of the $2q$ dispersion sheets there will be q wave vectors extending towards the corresponding q reciprocal lattice points. Transverse to each wave vector there will be an electric vector amplitude having a unique or proper direction. For such a

[6] P. P. Ewald, Ann. Physik **49**, 117 (1916); **49**, 1 (1916); **54**, 519 (1917).

[7] M. von Laue, Ergeb. Exakt. Naturw., 133 (1931).

[8] This x_n is proportional to the ξ's in Refs. 2, 3, 5.

point on a dispersion sheet, all wave vectors starting from that point, together with the amplitude directions and their relative magnitudes, constitute a mode of propagation. We may say that, in this sense, each wave point represents a mode of propagation.

In order to determine the amplitudes of the electric vectors in terms of the incident amplitude, and eventually to determine the intensities, we have to resort to the boundary conditions. In the region of x-ray wavelengths the boundaries of the crystal do not affect the electric and magnetic vectors and they both vary continuously across the surface. For the wave vectors, however, the continuity of phase requires that the tangential components of the wave vectors be continuous across the boundary. This condition allows the normal to the crystal surface together with the direction of incidence to select the active wavepoints on the dispersion sheets.

From the above considerations it follows that the conditions on amplitudes of the electric displacement vectors are: for the direction of incidence,

$$\sum_{\alpha=1}^{2q} \mathbf{D}_0^{(\alpha)} = \mathbf{D}_0^{(i)} \tag{2.4a}$$

and for the diffracted beams, separately,

$$\sum_{\alpha=1}^{2q} \mathbf{D}_n^{(\alpha)} = 0 \quad n=1, 2, \cdots, q. \tag{2.4b}$$

Von Laue and Kato[4] have shown that after the diffracted waves have departed a few "*Pendellosung*" periods from the boundary, the intensity in any direction of diffraction $\mathbf{k}_n$ is computed from

$$I_n = \text{const} \sum_{\alpha=1}^{2q} [D_n^{(\alpha)}]^2.$$

This intensity is the result of space and time averaging of the Poynting vectors.

In order to employ Eqs. (2.4a) and (2.4b) it is necessary to know all the vector amplitudes, and these will be determined once all the modes of propagation are known. It is thus apparent that the basic problem in multiple diffraction is the determination of the modes of propagation.

2.2. Two Fields

When two reciprocal lattice points lie near the Ewald sphere the amplitude of waves traveling in the two associated directions will be appreciable. We refer to it as the two-field case. Its theory has been worked out in great detail by several authors and is well known.

Elsewhere[9,10] we have worked out the modes of propagation for two fields as an illustration of the method employed here, where three amplitudes are appreciable. The modes determined were those belonging to the diameter points of the dispersion sheets, i.e., for the instance when Bragg's law is obeyed exactly. We have reproduced these modes in Fig. 3. In this figure the directions of incidence and diffraction are given by the wave vectors $\mathbf{k}_O$ and $\mathbf{k}_H$, respectively.

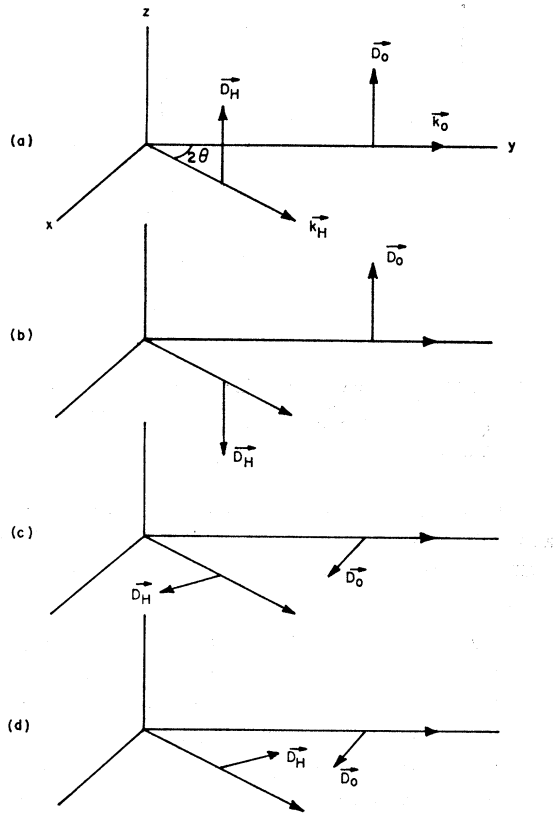

FIG. 3. Two-field modes of propagation. The modes shown correspond to the four symmetry points of the dispersion sheets. The plane of incidence is represented as the *xy* plane.

In any given Laue diffraction, when unpolarized radiation is incident, all four of these modes are excited and propagate; however, each has very different absorption properties. For example, it is well known that in the Borrmann effect for thick crystal plates ($\mu t > 10$) either the first or the second mode of Fig. 3, depending on the sign of the structure factor, survives the transmission. (For a thorough discussion of most of the above points see, for example, Ref. 5.)

We shall compute in the three-field case the modes of propagation for the diameter points in the same way as we have computed them for the two-field case.

2.3. The Three-Field Solution

The simplest case of simultaneous diffraction occurs when three reciprocal lattice points are close to the Ewald sphere. We will denote the three points by *O*, *H*,

[9] E. J. Saccocio and A. Zajac, Acta Cryst. **18**, 478 (1965).
[10] E. J. Saccocio, Ph.D. thesis, Polytechnic Institute of Brooklyn, 1964 (unpublished).

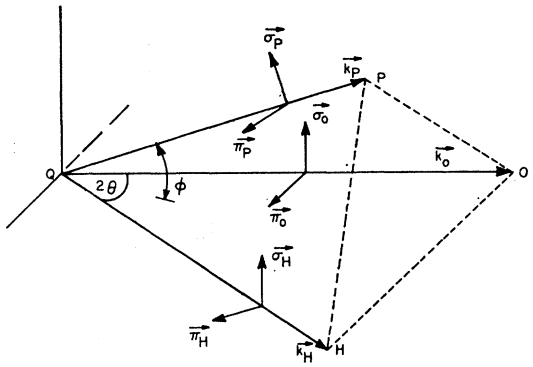

FIG. 4. Three-field geometry. Wave vectors $\mathbf{k}_O$, $\mathbf{k}_H$, and $\mathbf{k}_P$ make equal angles with one another. Reciprocal points on Ewald sphere are 000, 220, and 202. Unit vectors $\boldsymbol{\sigma}$ and $\boldsymbol{\pi}$ form mutually orthogonal set with respective wave vector.

and P and refer to this type of simultaneous diffraction as the three-field case. Because we wish to consider the possibility of simultaneous anomalous transmission, the choice of both the primary (H) and the secondary (P) diffraction is limited to those exhibiting the effect of anomalous transmission separately. The reflections which we actually consider correspond to $H=220$ and $P=202$ in a germanium crystal. This is therefore a rather special case where OHP forms an equilateral triangle in reciprocal space. The geometry is shown in Fig. 4. The unit vectors $\boldsymbol{\pi}_O$ and $\boldsymbol{\pi}_H$ lie in the QOH plane and the vector $\boldsymbol{\pi}_P$ is parallel to this plane. It will be recalled that each pair of unit vectors specify axes along which components of the respective vector amplitudes are taken, while the specification of their directions is arbitrary and is chosen according to the convenience of manipulation.

a. The Field Equations and the Secular Equation

For any three reciprocal lattice points O, H, P, the general set of equations (2.2) reduces to the following six equations:

$$
\begin{aligned}
-x_O D_O^{\sigma} &= 0 + 0 + \phi_{\bar{H}}(\boldsymbol{\sigma}_O\cdot\boldsymbol{\sigma}_H)D_H^{\sigma} + \phi_{\bar{H}}(\boldsymbol{\sigma}_O\cdot\boldsymbol{\pi}_H)D_H^{\pi} + \phi_{\bar{P}}(\boldsymbol{\sigma}_O\cdot\boldsymbol{\sigma}_P)D_P^{\sigma} + \phi_{\bar{P}}(\boldsymbol{\sigma}_O\cdot\boldsymbol{\pi}_P)D_P^{\pi}\\
-x_O D_O^{\pi} &= 0 + 0 + \phi_{\bar{H}}(\boldsymbol{\pi}_O\cdot\boldsymbol{\sigma}_H)D_H^{\sigma} + \phi_{\bar{H}}(\boldsymbol{\pi}_O\cdot\boldsymbol{\pi}_H)D_H^{\pi} + \phi_{\bar{P}}(\boldsymbol{\pi}_O\cdot\boldsymbol{\sigma}_P)D_P^{\sigma} + \phi_{\bar{P}}(\boldsymbol{\pi}_O\cdot\boldsymbol{\pi}_P)D_P^{\pi}\\
-x_H D_H^{\sigma} &= \phi_H(\boldsymbol{\sigma}_H\cdot\boldsymbol{\sigma}_O)D_O^{\sigma} + \phi_H(\boldsymbol{\sigma}_H\cdot\boldsymbol{\pi}_O)D_O^{\pi} + 0 + 0 + \phi_{H-P}(\boldsymbol{\sigma}_H\cdot\boldsymbol{\sigma}_P)D_P^{\sigma} + \phi_{H-P}(\boldsymbol{\sigma}_H\cdot\boldsymbol{\pi}_P)D_P^{\pi}\\
-x_H D_H^{\pi} &= \phi_H(\boldsymbol{\pi}_H\cdot\boldsymbol{\sigma}_O)D_O^{\sigma} + \phi_H(\boldsymbol{\pi}_H\cdot\boldsymbol{\pi}_O)D_O^{\pi} + 0 + 0 + \phi_{H-P}(\boldsymbol{\pi}_H\cdot\boldsymbol{\sigma}_P)D_P^{\sigma} + \phi_{H-P}(\boldsymbol{\pi}_H\cdot\boldsymbol{\pi}_P)D_P^{\pi}\\
-x_P D_P^{\sigma} &= \phi_P(\boldsymbol{\sigma}_P\cdot\boldsymbol{\sigma}_O)D_O^{\sigma} + \phi_P(\boldsymbol{\sigma}_P\cdot\boldsymbol{\pi}_O)D_O^{\pi} + \phi_{P-H}(\boldsymbol{\sigma}_P\cdot\boldsymbol{\sigma}_H)D_H^{\sigma} + \phi_{P-H}(\boldsymbol{\sigma}_P\cdot\boldsymbol{\pi}_H)D_H^{\pi} + 0 + 0\\
-x_P D_P^{\pi} &= \phi_P(\boldsymbol{\pi}_P\cdot\boldsymbol{\sigma}_O)D_O^{\sigma} + \phi_P(\boldsymbol{\pi}_P\cdot\boldsymbol{\pi}_O)D_O^{\pi} + \phi_{P-H}(\boldsymbol{\pi}_P\cdot\boldsymbol{\sigma}_H)D_H^{\sigma} + \phi_{P-H}(\boldsymbol{\pi}_P\cdot\boldsymbol{\pi}_H)D_H^{\pi} + 0 + 0
\end{aligned}
\tag{2.5}
$$

In the present case $H=220$ and $P=202$ in germanium, therefore

$$\phi_{\bar{H}}=\phi_H;\quad \phi_{H-P}=\phi_{P-H};\quad \phi_{\bar{P}}=\phi_P \tag{2.6}$$

and

$$\phi_P=\phi_H;\quad \phi_{H-P}=-\phi_H;\quad \phi_H=-|\phi_H|\,.$$

The various dot products appearing in (2.5) are

$$
\begin{aligned}
\boldsymbol{\sigma}_O\cdot\boldsymbol{\pi}_H=\boldsymbol{\sigma}_H\cdot\boldsymbol{\pi}_O=\boldsymbol{\sigma}_O\cdot\boldsymbol{\pi}_P=\boldsymbol{\sigma}_H\cdot\boldsymbol{\pi}_P &= 0\\
\boldsymbol{\sigma}_P\cdot\boldsymbol{\pi}_O &= \sin\theta\sin\phi \equiv \gamma_4\\
\boldsymbol{\sigma}_P\cdot\boldsymbol{\pi}_H &= -\sin\theta\sin\phi = -\gamma_4\\
\boldsymbol{\sigma}_O\cdot\boldsymbol{\sigma}_P=\boldsymbol{\sigma}_H\cdot\boldsymbol{\sigma}_P &= \cos\phi \equiv \gamma_3\\
\boldsymbol{\pi}_P\cdot\boldsymbol{\pi}_O=\boldsymbol{\pi}_P\cdot\boldsymbol{\pi}_H &= \cos\theta \equiv \gamma_2\\
\boldsymbol{\pi}_O\cdot\boldsymbol{\pi}_H &= \cos 2\theta \equiv \gamma\,,
\end{aligned}
\tag{2.7}
$$

where θ and ϕ are the angles shown in Fig. 4. Also, it can be shown readily that, in terms of γ,

$$\gamma_4^2=\frac{(1+2\gamma)(1-\gamma)^2}{2(1+\gamma)};\quad \gamma_3^2=\frac{2\gamma^2}{1+\gamma};\quad 2\gamma_2^2=1+\gamma.$$

The general three-field secular equation corresponding to Eqs. (2.5) is

$$
\begin{vmatrix}
x_O & 0 & \phi_{\bar{H}}(\boldsymbol{\sigma}_O\cdot\boldsymbol{\sigma}_H) & \phi_{\bar{H}}(\boldsymbol{\sigma}_O\cdot\boldsymbol{\pi}_H) & \phi_{\bar{P}}(\boldsymbol{\sigma}_O\cdot\boldsymbol{\sigma}_P) & \phi_{\bar{P}}(\boldsymbol{\sigma}_O\cdot\boldsymbol{\pi}_P)\\
0 & x_O & \phi_{\bar{H}}(\boldsymbol{\pi}_O\cdot\boldsymbol{\sigma}_H) & \phi_{\bar{H}}(\boldsymbol{\pi}_O\cdot\boldsymbol{\pi}_H) & \phi_{\bar{P}}(\boldsymbol{\pi}_O\cdot\boldsymbol{\sigma}_P) & \phi_{\bar{P}}(\boldsymbol{\pi}_O\cdot\boldsymbol{\pi}_P)\\
\phi_H(\boldsymbol{\sigma}_H\cdot\boldsymbol{\sigma}_O) & \phi_H(\boldsymbol{\sigma}_H\cdot\boldsymbol{\pi}_O) & x_H & 0 & \phi_{H-P}(\boldsymbol{\sigma}_H\cdot\boldsymbol{\sigma}_P) & \phi_{H-P}(\boldsymbol{\sigma}_H\cdot\boldsymbol{\pi}_P)\\
\phi_H(\boldsymbol{\pi}_H\cdot\boldsymbol{\sigma}_O) & \phi_H(\boldsymbol{\pi}_H\cdot\boldsymbol{\pi}_O) & 0 & x_H & \phi_{H-P}(\boldsymbol{\pi}_H\cdot\boldsymbol{\sigma}_P) & \phi_{H-P}(\boldsymbol{\pi}_H\cdot\boldsymbol{\pi}_P)\\
\phi_P(\boldsymbol{\sigma}_P\cdot\boldsymbol{\sigma}_O) & \phi_P(\boldsymbol{\sigma}_P\cdot\boldsymbol{\pi}_O) & \phi_{P-H}(\boldsymbol{\sigma}_P\cdot\boldsymbol{\sigma}_H) & \phi_{P-H}(\boldsymbol{\sigma}_P\cdot\boldsymbol{\pi}_H) & x_P & 0\\
\phi_P(\boldsymbol{\pi}_P\cdot\boldsymbol{\sigma}_O) & \phi_P(\boldsymbol{\pi}_P\cdot\boldsymbol{\pi}_O) & \phi_{P-H}(\boldsymbol{\pi}_P\cdot\boldsymbol{\sigma}_H) & \phi_{P-H}(\boldsymbol{\pi}_P\cdot\boldsymbol{\pi}_H) & 0 & x_P
\end{vmatrix}
=0. \tag{2.8}
$$

Using relations (2.6) and (2.7), and writing the parameter x in units of $|\phi_H|$, and factoring out $|\phi_H|$,[11] the secular equation reduces to

$$\begin{vmatrix} -x_O & 0 & 1 & 0 & \gamma_3 & 0 \\ 0 & -x_O & 0 & \gamma & \gamma_4 & \gamma_2 \\ 1 & 0 & -x_H & 0 & -\gamma_3 & 0 \\ 0 & \gamma & 0 & -x_H & \gamma_4 & -\gamma_2 \\ \gamma_3 & \gamma_4 & -\gamma_3 & \gamma_4 & -x_P & 0 \\ 0 & \gamma_2 & 0 & -\gamma_2 & 0 & -x_P \end{vmatrix} = 0. \quad (2.9)$$

We assume that the surface of the crystal is cut parallel to the plane of the reciprocal triangle OHP shown in Fig. 4.[12] Such a choice of the surface of the crystal plate allows a unidirectional incident beam to select simultaneously the diameter points on all the dispersion sheets. The diffractions are then perfectly symmetrical and all diffracting atomic planes, including the difference $(H-P)$ planes, are normal to the crystal surface.

Assuming then that the normal is in the correct position to excite the diameter points, one determines the corresponding values by simply setting x_O, x_H, and x_P equal in Eq. (2.9) and solving. To gain more insight and perhaps some additional information, a less straightforward procedure is of advantage. In an experimental arrangement involving simultaneous diffraction, one usually maintains a given diffraction at its peak and rotates the crystal so that other diffractions may take place. From the point of view of the dispersion sheets this is translated to mean that x_O and x_H are kept equal, while x_P is left to vary in accordance with its permitted values. Therefore, in Eq. (2.9) we set $x_O=x_H=x$ and leave x_P as it is. The secular equation now can be written

$$(x-1)[x_P(x+\gamma)-2\gamma_2^2] \times\{(x+1)[x_P(x-\gamma)-2\gamma_4^2]-2\gamma_3^2(x-\gamma)\}=0. \quad (2.10)$$

It is obvious from (2.10) that $x=+1$ is a solution, but most important, it is independent of x_P. The significance of this, as we shall see below, is that the third field, or more loosely, the additional reciprocal lattice point, cannot affect this diameter point. It is important to note that the factor $(x-1)$ in Eq. (2.10) will always appear from the secular equation (2.8) for any three-field situation as long as $\phi_P=\pm\phi_{H-P}$ a condition necessary for three fields in most crystal space groups. Further, from Eq. (2.10) as $x_P\rightarrow\infty$ it can be seen that in this limit, since three fields reduce to two, the diameter values must become the four of the two-field case, namely, $x=\pm1$ and $x=\pm\gamma$; and in fact they do. We see that we have a two-field solution as at least one of the solutions in the three-field case.

To determine the diameter values in the three-field case we now set x_P equal to x in Eq. (2.10), and solving what has become a characteristic equation, we obtain the eigenvalues,

$$\begin{aligned} x_1&=-(1-2\gamma), \\ x_{2,3}&=-(1+\gamma), \\ x_{4,5,6}&=+1.[13] \end{aligned} \quad (2.11)$$

The multiplicity of the second and third eigenvalues indicates the existence of degeneracies and, except for the unique value x_1, precludes a straightforward analysis of the modes of propagation.

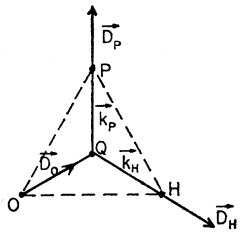

FIG. 5. The unique mode of propagation.

b. *The Modes of Propagation*

For any value x_i given by Eq. (2.11) satisfying the characteristic equation (2.9), the number of independent homogeneous equations [given by Eqs. (2.5)], is $(N-m)$, where N is the total number of homogeneous equations and m is the multiplicity of the root. For the unique eigenvalue x_1 of the set (2.11) we obtain from Eqs. (2.5) five independent equations which are sufficient to solve for the five unknown ratios. These equations written in units of $|\phi_H|$ are:

$$\begin{aligned} -x_1D_O^\sigma+D_H^\sigma+\gamma_3D_P^\sigma&=0, \\ -x_1D_O^\pi+\gamma D_H^\pi+\gamma_4D_P^\sigma+\gamma_2D_P^\pi&=0, \\ D_O^\sigma-x_1D_H^\sigma-\gamma_3D_P^\sigma&=0, \\ \gamma D_O^\pi-x_1D_H^\pi+\gamma_4D_P^\sigma-\gamma_2D_P^\pi&=0, \\ \gamma_2D_O^\pi-\gamma_2D_H^\pi-x_1D_P^\pi&=0. \end{aligned} \quad (2.12)$$

From these we obtain the ratios:

$$\frac{D_O^\sigma}{D_O^\pi}=\frac{-1}{(1+2\gamma)^{\frac{1}{2}}}, \quad \frac{D_H^\sigma}{D_H^\pi}=\frac{1}{(1+2\gamma)^{\frac{1}{2}}}, \quad \frac{D_P^\pi}{D_P^\sigma}=0, \quad (2.13)$$

and

$$|\mathbf{D}_P|=|\mathbf{D}_H|=|\mathbf{D}_O|.$$

This mode is represented in Fig. 5. The figure is a three-dimensional representation: Q is the center of the Ewald sphere, and from Q originate the three wave vectors $\mathbf{k}_O$, $\mathbf{k}_H$, and $\mathbf{k}_P$, which terminate at the reciprocal lattice points O, H, and P on the surface of the sphere. Every pair of these wave vectors defines a plane and the three

[11] That is, $x_O=(|\phi_H|/|\phi_H|)x_O=|\phi_H|x_O'$ etc., then drop the prime in Eq. (2.9).

[12] This configuration is considered throughout the entire paper.

[13] The eigenvalues evaluated here are specifically for the $H=220$ and $P=20\bar{2}$ simultaneous reflections. It can be shown that these eigenvalues are independent of the choice of equivalent sets of reciprocal lattice points such as $H=2\bar{2}0$, $P=202$, or $H=\bar{2}20$, $P=\bar{2}02$.

resulting planes are inclined at equal angles (β) to each other [the angle β is given by $\cos\beta=\gamma/(1+\gamma)$]. The electric vectors $\mathbf{D}_O$, $\mathbf{D}_H$, $\mathbf{D}_P$ bisect these angles and are respectively perpendicular to the wave vectors $\mathbf{k}_O$, $\mathbf{k}_H$, $\mathbf{k}_P$.

As a matter of interest, it will be noticed that the plane of vibration for each vector is parallel to a respective difference (atomic) plane; e.g., $\mathbf{D}_P$ lies in a plane parallel to $(H-O)$ plane.

We will next investigate the triply degenerate mode, i.e., the one corresponding to the last eigenvalue from the set given by (2.11). In this case the set (2.5) yields three independent homogeneous equations only. It becomes necessary therefore to resort to a perturbation to remove the existing degeneracy. The perturbation consists in allowing the reciprocal lattice point P to move away from the Ewald sphere, while keeping O and H fixed on the sphere. This is equivalent to rotating the crystal about the diffraction vector $\mathbf{H}$. We have seen above that, with respect to the dispersion sheets, this means that the two parameters x_O and x_H remain equal, while x_P takes on its allowed value going to infinity as P leaves the sphere completely. Of course, we have already seen this perturbed characteristic equation, namely,

$$(x-1)[x_P(x+\gamma)-2\gamma_2^2]\times\{(x+1)[x_P(x-\gamma)-2\gamma_4^2]-2\gamma_3^2(x-\gamma)\}=0. \quad (2.14)$$

However, now it takes on a somewhat different hue in the light of this treatment. We note that the eigenvalue $x=1$ not only remains unchanged but is now unique and is independent of x_P. This means that $x=1$ continues to be a solution regardless of the position of the reciprocal lattice point P with respect to the Ewald sphere. The associated mode of propagation can therefore be determined uniquely from the set (2.5) and is not influenced by the presence of the third field. It turns out that in this case

$$D_O^{\pi}/D_O^{\sigma}=0,\quad D_H^{\pi}/D_H^{\sigma}=0,\quad D_P^{\sigma}=0,\quad D_P^{\pi}=0,\quad |\mathbf{D}_O|=|\mathbf{D}_H|. \quad (2.15)$$

This mode is shown in Fig. 6(a). It should be noticed that it is identical to one of the two field modes. This could have been predicted since the eigenvalue is exactly the same as in the two-field case.

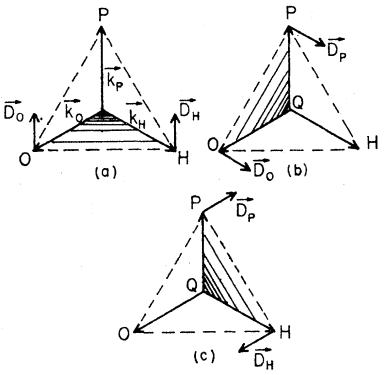

FIG. 6. Triply degenerate modes of propagation. Note that the third amplitude is zero in each.

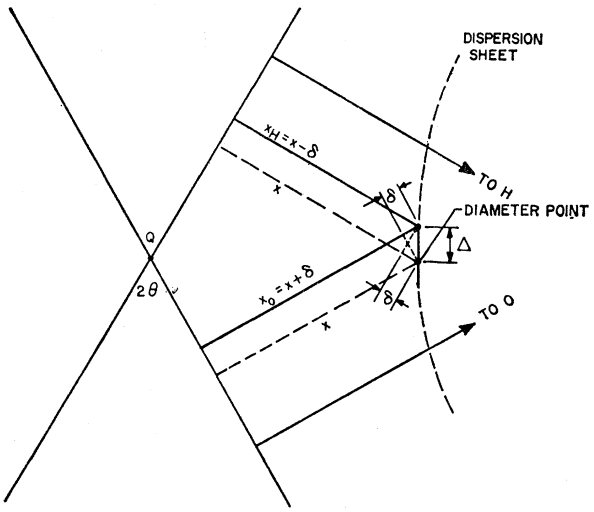

FIG. 7. Representation of the perturbation along the dispersion sheet off diameter point.

So far, only one mode corresponding to the triple root $x=1$ has been determined. Additional perturbations would be required to remove the remaining ambiguities, but are not actually necessary to carry through if we take advantage of the symmetry of the three reciprocal lattice points. That is, if we permute the indices O, H, P in the perturbation, we can obtain the results. These modes are of the same kind as the one already obtained, except possibly for the phase of the electric vectors. Since the sign of ϕ_P is the same as that of ϕ_H, the phases of the (O,H) and (O,P) modes are identical. Figure 6(b) gives the second mode. However, ϕ_{H-P} is the negative of ϕ_H, and this requires the phase shown in Fig. 6(c).

In the case of the doubly degenerate mode, which corresponds to the second eigenvalue of the set given by Eqs. (2.11), another type of perturbation is required. In the perturbation applied before, O and H were held on the Ewald sphere and P was moved away from it. The secular equation (2.14) resulted. If we substitute in the square bracket of Eq. (2.14), $x=-(1+\gamma)$, equate this bracket to zero and solve for x_P, we obtain $x_P=-(1+\gamma)$. A similar procedure applied to the curly brackets again yields $x_P=-(1+\gamma)$. The degeneracy thus remains.

As shown in Fig. 7 the new perturbation will consist in moving away from those points on the dispersion sheets where x_O and x_H are equal, and keeping x_P equal to its diameter value. Thus we let

$$x_O=x+\delta,\quad x_H=x-\delta,\quad x_P=x, \quad (2.16)$$

where δ will be kept so small that second-order terms in δ can be neglected. The independent equations from

the set (2.5) now become

$$\begin{aligned}
-(x+\delta)D_O^{\sigma}+D_H^{\sigma}+\gamma_3 D_P^{\sigma}&=0,\\
-(x+\delta)D_O^{\pi}+\gamma D_H^{\pi}+\gamma_4 D_P^{\sigma}+\gamma_2 D_P^{\pi}&=0,\\
D_O^{\sigma}-(x-\delta)D_H^{\sigma}-\gamma_3 D_P^{\sigma}&=0,\\
\gamma D_O^{\pi}-(x-\delta)D_H^{\pi}+\gamma_4 D_P^{\sigma}-\gamma_2 D_P^{\pi}&=0,\\
\gamma_3 D_O^{\sigma}+\gamma_4 D_O^{\pi}-\gamma_3 D_H^{\sigma}+\gamma_4 D_H^{\pi}-xD_P^{\sigma}&=0,
\end{aligned} \tag{2.17}$$

where x has the value $-(1+\gamma)$. [Equations (2.17) are also independent for the eigenvalue $-(1-2\gamma)$ but not for $x=1$.] From Eqs. (2.17) we obtain the following ratios of the components of the electric displacement vectors which describe this mode:

$$\begin{aligned}
&\frac{D_O^{\pi}}{D_O^{\sigma}}=\frac{1-\gamma}{2(1+2\gamma)^{\frac{1}{2}}}\equiv\tan\omega,\\
&\frac{D_H^{\pi}}{D_H^{\sigma}}=\frac{-(1-\gamma)}{2(1+2\gamma)^{\frac{1}{2}}};\quad \frac{D_P^{\pi}}{D_P^{\sigma}}=0,\\
&|\mathbf{D}_H|=|\mathbf{D}_O|,\\
&|\mathbf{D}_P|=\left[\frac{2(1+2\gamma)}{5+\gamma}\right]^{\frac{1}{2}}|\mathbf{D}_O|.
\end{aligned} \tag{2.18}$$

This mode is shown in Fig. 8(a) and corresponds to the diameter point and also its immediate vicinity.

Since in our case the reciprocal points P and H are indistinguishable, the remaining mode will be similar to that shown in Fig. 8(a) but the roles of H and P will be interchanged; this mode is shown in Fig. 8(b).

The modes shown in Figs. 8(a) and 8(b) are unusual in the sense that they could not have been predicted by intuition, or from arguments of symmetry.

c. The Boundary Conditions

Having thus determined the modes of propagation, we are now in a position to use the boundary conditions to calculate the vector amplitudes $\mathbf{D}_n^{\alpha}$ in terms of an input amplitude $\mathbf{D}_O^{(i)}$, and thus the corresponding intensities.

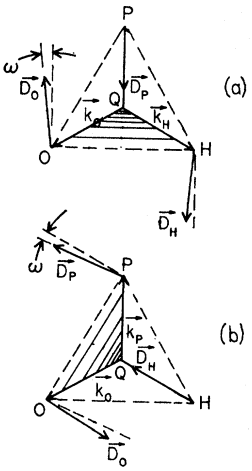

FIG. 8. Doubly degenerate modes of propagation. (a) The dashed parallel lines are perpendicular to the "plane of incidence" lined in. The angle by which $\mathbf{D}_O$ or $\mathbf{D}_H$ deviates from the perpendicular is indicated by ω. The vector $\mathbf{D}_P$ lies on the bisector of the angle between planes, transverse to $\mathbf{k}_P$ (not shown). (b) The same mode as in Fig. 8(a) with role of P and H interchanged.

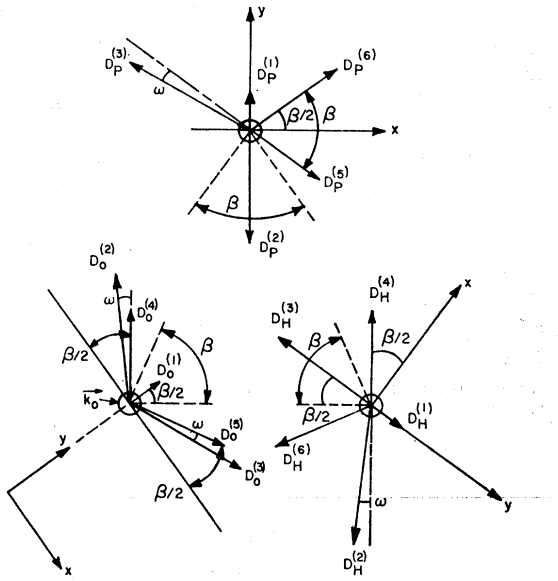

FIG. 9. Modes of propagation superposed. Wave vectors are represented perpendicular to plane of diagram. True projection of angles between amplitudes. Superscripts are as follows: (1), unique mode; (2), (3), doubly degenerate mode; (4), (5), (6), triply degenerate mode. Input directions at $\mathbf{k}_O$ of polarization along x and y.

It is to be realized at this point that those wave vectors originating from the $2q$ dispersion sheets (six in the present case) and terminating at the same reciprocal lattice point, all have slightly different magnitudes and directions (except in cases of degeneracy when they are identical). These vectors will be said to compose a beam. In applying the boundary conditions, the small differences in the directions of the wave vectors in a beam are neglected and the electric vector amplitudes from each mode belonging to the same beam are superimposed. In Fig. 9 each beam (simply labeled k_q, etc.) is assumed to be perpendicular to the plane of the paper. Such a construction is desirable since we shall be adding vector amplitudes belonging to the same beam. The numerical superscripts (α) attached to the amplitudes have been assigned according to the following scheme:

(1), the unique mode,

(2), (3), the doubly degenerate mode,

(4), (5), (6), the triply degenerate mode.

The angle ω has been defined in Eq. (2.18) and β is the angle between planes formed by pairs of wave vectors.

Unpolarized incident radiation consists of two components unrelated in phase, and linearly polarized at right angles to each other. The x and y directions shown in Fig. 9 at $\mathbf{k}_O$ are the assumed directions of polarization of each component. All the electric vectors belonging to the beam $\mathbf{k}_O$ will be resolved along the x and y directions

indicated at $\mathbf{k}_O$. Since for each direction of diffraction ($\mathbf{k}_H$ and $\mathbf{k}_P$) the sum of the amplitudes must be zero at the boundary independently of the assumed input directions of polarization, we arbitrarily chose the convenient x and y directions indicated at H and P in Fig. 9 and resolved along them all the corresponding amplitudes. Two separate evaluations are necessary: one for an incident beam linearly polarized along y, and subsequently a second for an incident beam polarized along the x direction.

The incident amplitudes will be denoted by $D_{Ox}{}^{(i)}$ and $D_{Oy}{}^{(i)}$. The boundary conditions given by Eqs. (2.4a) and (2.4b), written in a manner applicable to the case of an incident beam linearly polarized along the y direction, are, for the incident beam

$$\sum D_{Ox}{}^{(\alpha)}=0, \quad \sum D_{Oy}{}^{(\alpha)}=D_{Oy}{}^{(i)}, \tag{2.19}$$

and for the diffracted beams.

$$\sum D_{nx}{}^{(\alpha)}=0, \quad \sum D_{ny}{}^{(\alpha)}=0 \qquad n=H,P. \tag{2.20}$$

For brevity we will introduce the following symbols:

$$\begin{aligned} A&=\sin(\beta/2-\omega),\\ B&=\cos(\beta/2-\omega),\\ C&=\sin(\beta/2),\\ D&=\cos(\beta/2). \end{aligned} \tag{2.21}$$

Applying the boundary conditions expressed by Eqs. (2.19) and (2.20) for the incident and diffracted beams we obtain:

$$\begin{aligned}
k_O:\ x\text{ component:}&\quad 0=-BD_O{}^{(2)}+BD_O{}^{(3)}-DD_O{}^{(4)}-DD_O{}^{(5)} && \text{(a)}\\
y\text{ component:}&\quad D_{Oy}{}^{(i)}=D_O{}^{(1)}+AD_O{}^{(2)}+AD_O{}^{(3)}+CD_O{}^{(4)}+CD_O{}^{(5)} && \text{(b)}\\
k_P:\ x\text{ component:}&\quad 0=-BD_P{}^{(3)}+DD_P{}^{(5)}+DD_P{}^{(6)} && \text{(c)}\\
y\text{ component:}&\quad 0=D_P{}^{(1)}+AD_P{}^{(3)}-D_P{}^{(2)}-CD_P{}^{(5)}+CD_P{}^{(6)} && \text{(d)}\\
k_H:\ x\text{ component:}&\quad 0=-BD_H{}^{(2)}+DD_H{}^{(4)}-DD_H{}^{(6)} && \text{(e)}\\
y\text{ component:}&\quad 0=D_H{}^{(1)}+AD_H{}^{(2)}-D_H{}^{(3)}-CD_H{}^{(4)}-CD_H{}^{(6)}. && \text{(f)}
\end{aligned} \tag{2.22}$$

The relative magnitudes of the vector amplitudes $\mathbf{D}_O$, $\mathbf{D}_H$, and $\mathbf{D}_P$ are known from the modal results, as follows:

From the last line of Eqs. (2.13) we have for the unique mode ($\alpha=1$)

$$D_H{}^{(1)}=D_P{}^{(1)}=D_O{}^{(1)}, \tag{2.23}$$

and from (2.18), in which $\alpha=2, 3$,

$$D_H{}^{(2)}=D_O{}^{(2)}; \quad D_P{}^{(2)}=bD_O{}^{(2)},$$

and

$$D_H{}^{(3)}=bD_O{}^{(3)}; \quad D_P{}^{(3)}=D_O{}^{(3)},$$

where

$$b=\left[\frac{2(1+2\gamma)}{5+\gamma}\right]^{\frac{1}{2}}, \tag{2.24}$$

which may also be shown to be equal to $2A$ defined in Eq. (2.21).

From Eq. (2.15) we also have

$$D_H{}^{(4)}=D_O{}^{(4)}; \quad D_P{}^{(5)}=D_O{}^{(5)}; \quad D_P{}^{(6)}=D_H{}^{(6)}. \tag{2.25}$$

Substitution of Eqs. (2.23), (2.24), and (2.25) into Eqs. (2.22) yields six equations in six unknowns [five D_O's plus $D_H{}^{(6)}$]. The solution of these equations completes the first half of the task. The entire procedure is then repeated using the x components of the input amplitude. The results for the unknowns are contained in the following table with the incident amplitudes $D_{Ox}{}^{(i)}$ and $D_{Oy}{}^{(i)}$ taken as unity.

The particular case which we are considering is that of the 220 and 202 reflections from germanium with copper characteristic radiation (1.54A). For this case ω, defined by the first of relations (2.18), is 6° 30′. Evaluating the various amplitudes in Table I, and utilizing the relations (2.23), (2.24), and (2.25), yields Tables II and III. (The minus signs in Table III indicate a reversal of those directions shown in Fig. 9.) In addition to the amplitudes, these tables also contain the squares

TABLE I. Magnitudes of vector amplitudes.[a]

	x input	y input
$HD_O{}^{(1)}$:	0	$-6D(AD+BC)^2$
$HD_O{}^{(2)}$:	$6CD(AD+BC)$	$-6D^2(AD+BC)^2$
$HD_O{}^{(3)}$:	$-6CD(AD+BC)$	$-6D^2(AD+BC)$
$HD_O{}^{(4)}$:	$3(AD+BC)(3AD+BC)$	$-6BD(AD+BC)$
$HD_O{}^{(5)}$:	$-3(AD+BC)(3AD+BC)$	$-6BD(AD+BC)$
$HD_H{}^{(6)}$:	$3(AD+BC)(3AD-BC)$	0

[a] $H=-18D(AD+BC)^2$.

TABLE II. Incident beam polarized along y.

α	$D_O{}^{(\alpha)}$	$[D_O{}^{(\alpha)}]^2$	$D_H{}^{(\alpha)}$	$[D_H{}^{(\alpha)}]^2$	$D_P{}^{(\alpha)}$	$[D_P{}^{(\alpha)}]^2$	$\sum_q [D_q{}^{(\alpha)}]^2$
1	0.333	0.111	0.333	0.111	0.333	0.111	0.333
2	0.323	0.086	0.323	0.105	0.297	0.105	0.296
3	0.323		0.297		0.323		...
4	0.344	0.139	0.344	0.118	0	0	0.257
5	0.344		0	0	0.344	0.118	0.118
6	0	0	0	0	0	0	0
							$\Sigma=1.004$

of the amplitudes, and the sums of the squares. Where the curly brackets appear, the bracketed amplitudes have first been vector-added and then squared since these amplitudes belong to degenerate modes.

d. Comparison of Three- with Two-Field Intensities

In the ordinary situation of single diffraction, assuming an unpolarized incident radiation, each of the four modes of propagation receives an equal share of the incident intensity. Since there are two amplitudes per mode, each amplitude represents 12.5% of the total intensity.[14] This is true independently of which diffraction is considered. In a three-field diffraction this is not so and the distribution of intensities depends on the third reciprocal lattice point. For the specific case above, from Tables II and III, the distribution of intensity among the beams becomes 43.4% for the $\mathbf{k}_O$ beam and 28.3% for each of the two remaining beams $\mathbf{k}_P$ and $\mathbf{k}_H$. In either the two- or the three-field case these intensity values are those at the entrance surface of the crystal, and since in general each mode of propagation has very different absorption coefficients, the exit intensities are not simply proportionate. In two-field diffraction, of the two sigma modes (a and b of Fig. 3) one has nodes of the electric field in the atomic planes, while the other has its antinodes in these planes, resulting in, respectively, an anomalously low and high absorption. For the remaining so called π modes, because neither has true nulls, the absorption is such that in thick crystals (wherein the Borrmann effect is considered) neither survives a transmission. Thus, in an anomalous transmission at most 25% of the incident intensity will survive with half in each of the two directions.

In the three-field case above, the triply degenerate mode (Fig. 6) is the identical, anomalously low-absorbing two-field mode, containing only two nonzero amplitudes, i.e., the third amplitude is zero in each. These three therefore will transmit anomalously. Considering the modes 4, 5, and 6 of Tables II and III, we find that in such a multi-Borrmann effect the anomalously transmitted intensity is 50.05%, with unequal shares of 11.7% for each reflected-diffracted beam and 26.65% for the forward-diffracted beams. From the experimental point of view this means that in monitoring the two beams (forward and reflected) in an anomalous transmission, when the third reciprocal lattice point is brought onto the Ewald sphere, only a small change is expected in the reflected beam (from 12.5% to 11.7%) while a large increase (from 12.5% to 26.7%) should take place in the forward beam.

In the Tables II and III, the incident beam intensity is normalized to unity for each direction of polarization, and it can be seen directly what differences there would be in polarized experiments conforming to these directions. It is evident here that the simple splitting of polarization directions in ordinary two-field diffraction cannot be expected in multiple diffraction.

TABLE III. Incident beam polarized along x.

α	$D_O^{(\alpha)}$	$[D_O^{(\alpha)}]^2$	$D_H^{(\alpha)}$	$[D_H^{(\alpha)}]^2$	$D_P^{(\alpha)}$	$[D_P^{(\alpha)}]^2$	$\sum_q [D_q^{(\alpha)}]^2$
1	0	0	0	0	0	0	0
2	−0.209	0.138	−0.209	0.116	−0.192	0.116	0.370
3	0.209		0.192		0.209		...
4	−0.373	0.394	−0.373	0.116	0		0.510
5	0.373		0		0.373	0.116	0.116
6	0	0	−0.152		−0.152		...
							$\Sigma = 0.996$

[14] For a more thorough analysis and explanation of this and subsequent items pertinent to the two-field case see Ref. 5.

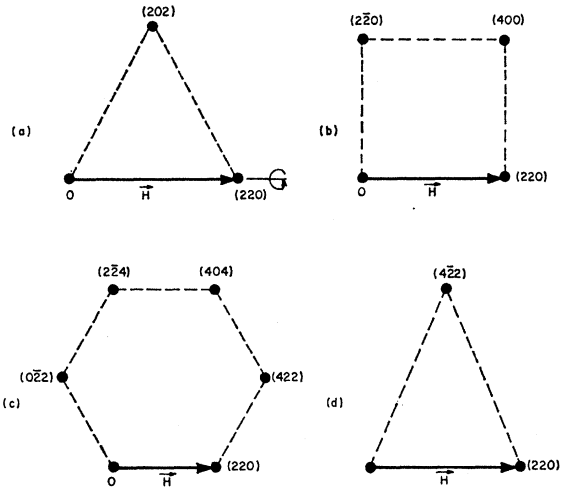

FIG. 10. Possible three-, four-, and six-field configurations.

3. EXPERIMENTS

All of our experiments were of the anomalous transmission type and were performed with an artificially grown germanium crystal of good quality (about 1000 dislocations per cm^2). The crystal was in the form of a circular plate, 2 cm in diameter and about 0.5 mm thick. In observing an ordinary Borrmann effect only one of the four modes of propagation survives such a crystal, whereas, in a three-field transmission we have seen that at least one of six will, and in our special case, due to the degeneracy, three survive. Thus anomalous transmission provides us with means of studying a lesser number of modes and thereby a more simplified propagation. The 220 planes provide the strongest anomalous transmission and for this reason were taken as the primary diffracting planes, which were perpendicular to the large face of the crystal. An axis of rotation was made coincident with the normal to these planes in order to effect the necessary conditions for multiple diffraction. That is, the crystal could be rotated about the primary reciprocal vector OH (marked H in Fig. 10) joining the origin O and the 220 point of the reciprocal lattice. Once this was achieved, the crystal could be rotated and simultaneous diffractions searched for. Simultaneous diffractions will occur when additional reciprocal lattice points enter the Ewald sphere. As shown in Fig. 10 there are four

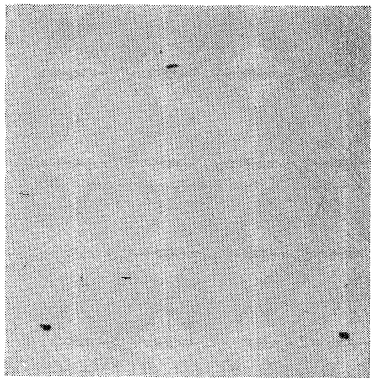

FIG. 11. Simultaneous anomalous transmission in germanium crystal. Unpolarized incident x-ray radiation. Lower left and right spots are, respectively, O and H beams. Upper spot, the P beam.

possibilities when strongest reflections simultaneous with 220 should be observed (i.e., in the sense of anomalous transmission). We concentrated on the three-field symmetrical case [Fig. 10(a)] having worked out the theory for that particular case.

As before, we will call the transmitted beam, the primary reflected beam, and the additional beam, the O, H, and P beams, respectively. In searching for simultaneous diffraction we could monitor the reflected beam H or the transmitted beam O, and look for changes of intensity. In our first investigations, with unpolarized filtered x rays of 1.54-Å wavelength, the H beam was monitored but no changes of intensity were observed. When the O beam was monitored and the crystal rotated about the OH vector, the entering of additional lattice points onto the Ewald sphere was signalled by a considerable increase of intensity of the O beam. In some cases the increase was 100%. Photographic exposure confirmed that in such cases the simultaneous diffraction did indeed occur. We obtained photographs of the three- and four-field cases, of which a reproduction of the three-field case is shown in Fig. 11.

A quantitative study of the three-field case was attempted by us, and it was obvious that for this we needed a monochromatic, polarized incident x-ray beam. Using a special device[15] we were able to obtain an x-ray beam which was both monochromatic and could be polarized in any desired direction. We performed several experiments with various directions of polarization. One of them was the x direction indicated in Fig. 9. In this case all three fields (O,H,P) were observed with the forward beam approximately three times as intense as H, and P about three quarters of H. This result should be compared with Table III where the intensities for the anomalously transmitting modes are nearly in the ratio 3:1:1.

These and other results which we have obtained are not in disagreement with our theoretical evaluations, but neither can they serve as their verification because of some uncertainty caused by the divergence of the incident beam. Reduction of the divergence produced in our case beams of such weak intensities that measurements were doubtful.

[15] H. Cole, F. W. Chambers, and C. G. Wood, Rev. Sci. Instr. 33, 435 (1962).

Further experiments are needed to verify the theoretical predictions fully. The main feature of these additional experiments will be a nondivergent, reasonably strong, and monochromatic incident x-ray beam.

4. DISCUSSION AND CONCLUSIONS

The general dynamical theory of x-ray diffraction requires that for q fields propagated in the crystal, the equations of the $2q$ dispersion sheets be obtained. Practically all the information concerning the characteristics of the x-ray wave field can be obtained from these equations. In the ordinary case of two fields, the dispersion sheets can be obtained in a relatively easy manner. In cases when more than two fields are present this becomes difficult and in general prohibitive. In order to preserve the analytical solution, and yet obtain the basic understanding of the multiple diffraction, we utilized *the diameter points of the dispersion sheets only. The solution of the problem was provided when the normal modes of propagation were evaluated.* This knowledge of the normal modes of propagation contains the essential and most important information for multiple diffraction.

In this paper we have treated only the highly symmetrical case of three fields in the germanium crystal. All the modes of propagation have been evaluated in a particular case, and it was established which of the modes are anomalously transmitted. Out of the possible six modes, only the three degenerate modes consisting of pairs of dynamically coupled fields can be anomalously transmitted.

In the two-field case, when anomalous transmission is possible, a pair of dynamically coupled fields is transmitted. We may thus say that in the three-field case, two-field solutions are present, and these provide the only modes which are anomalously transmitted.

Among the modes which we have determined, there is a unique mode consisting of three dynamically coupled fields, but this mode is anomalously absorbed.

As already stated, we have treated a special case of three fields. The extension of the theory to higher number of fields, and to asymmetric cases, has still to be performed.

In conclusion it may be remarked that the inherent beauty of the dynamical theory, so well illustrated in the two-field case, is also present when the number of fields is higher. We have considered a noncoplanar three-field case. In the two-field analysis the waves break up into two independent states of polarization. Nothing similar in the three-field analysis is possible, and as already stated, the modes of propagation are the fundamental quantities which provide the solution of the problem.

ACKNOWLEDGMENTS

We wish to acknowledge that the problem of investigating simultaneous anomalous transmission was suggested to us by P. P. Ewald. We thank J. P. Aldag for helpful discussions, and J. Bindell for assistance in the experiments.

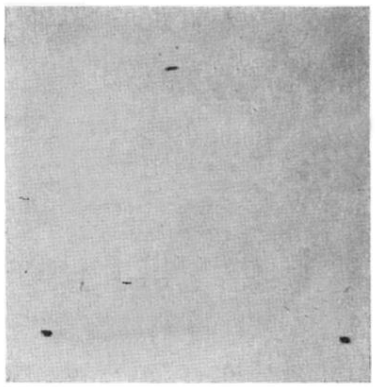

FIG. 11. Simultaneous anomalous transmission in germanium crystal. Unpolarized incident x-ray radiation. Lower left and right spots are, respectively, *O* and *H* beams. Upper spot, the *P* beam.